Visualization of trigeminal ganglion sensory neuronal signaling regulated by Cdk5

Minghan Hu[1], **Andrew D. Doyle**[2], **Kenneth M. Yamada**[2,*], **Ashok B. Kulkarni**[3,4,*]

[1]Functional Genomics Section and Cell Biology Section, National Institute of Dental and Craniofacial Research, National Institutes of Health, Bethesda, MD, USA

[2]Cell Biology Section, National Institute of Dental and Craniofacial Research, National Institutes of Health, Bethesda, MD, USA

[3]Functional Genomics Section, National Institute of Dental and Craniofacial Research, National Institutes of Health, 30 Convent Drive, MSC 4359, Bethesda, MD, USA

[4]Lead contact

SUMMARY

The mechanisms underlying facial pain are still incompletely understood, posing major therapeutic challenges. Cyclin-dependent kinase 5 (Cdk5) is a key neuronal kinase involved in pain signaling. However, the regulatory roles of Cdk5 in facial pain signaling and the possibility of therapeutic intervention at the level of mouse trigeminal ganglion primary neurons remain elusive. In this study, we use optimized intravital imaging to directly compare trigeminal neuronal activities after mechanical, thermal, and chemical stimulation. We then test whether facial inflammatory pain in mice could be alleviated by the Cdk5 inhibitor peptide TFP5. We demonstrate regulation of total Ca^{2+} intensity by Cdk5 activity using transgenic and knockout mouse models. In mice with vibrissal pad inflammation, application of TFP5 specifically decreases total Ca^{2+} intensity in response to noxious stimuli. It also alleviates inflammation-induced allodynia by inhibiting activation of trigeminal peripheral sensory neurons. Cdk5 inhibitors may provide promising non-opioid candidates for pain treatment.

Graphical Abstract

In brief

By using intravital live imaging to record mouse trigeminal ganglion neuronal activities in response to facial pain, Hu et al. demonstrate that Cdk5 regulates primary sensory neuronal pain signaling. In addition, a Cdk5 peptide inhibitor can suppress inflammation-induced pain signaling at the peripheral nervous system level.

INTRODUCTION

Facial and oral pain afflicts 5%–12% of the world's population and can severely decrease quality of life (Crandall, 2018; Herrero Babiloni et al., 2018) and contributes to problems such as the opioid crisis (Sugawara et al., 2019). Understanding trigeminal pain signal coding and transmission is paramount for the effective management of orofacial pain.

The trigeminal ganglion (TG) of the peripheral nervous system contains nociceptor cell bodies that innervate and contribute to pain sensing in the face and the oral cavity (Kim et al., 2014; Rothermel et al., 2011), transmitting pain sensation through the TG to the central nervous system (CNS) (Bista and Imlach, 2019). Both noxious and non-noxious stimuli can activate specific nociceptors in TG neurons. For example, transient receptor potential vanilloid type 1 (TRPV1) plays a key role in pain transmission of nociceptive information. TRPV1 is a calcium-permeable channel sensitive to stimuli such as thermal, chemical, and mechanical stimuli (Gonzalez-Ramirez et al., 2017; Julius, 2013; Warwick et al., 2019).

TRPV1 activity can be regulated by phosphorylation, which increases sensitivity to pain stimuli (Hall et al., 2018; Jendryke et al., 2016).

Cyclin-dependent kinase 5 (Cdk5) is a proline-directed serine/threonine kinase that is expressed ubiquitously (Hellmich et al., 1992; Liu et al., 2016). When bound to its activator, p35, Cdk5 phosphorylates target proteins for normal neuronal development and homeostasis (Cortes et al., 2019; Pareek et al., 2013). Cdk5 is also a key component of the nociceptive pathway, and its expression and activity increase upon inflammation following nociceptive stimulation (Pareek et al., 2006; Yang et al., 2007). Intrathecal administration of a Cdk inhibitor can both attenuate formalin-induced nociceptive responses and diminish morphine tolerance (Wang et al., 2004, 2005). Previously, our laboratory validated *in vivo* roles for Cdk5 in facial hypoalgesic or hyperalgesic behavior in transgenic mice with decreased or increased Cdk5 activity, respectively (Prochazkova et al., 2013).

Cdk5 phosphorylates TRPV1 at Thr-407 (mouse or human) (Liu et al., 2015) or Thr-406 (rat) (Pareek et al., 2007) to enhance channel function. Because Cdk5 is associated with pathology of inflammation and pain, pharmacological targeting of this kinase is an attractive potential pain therapy. However, the roles of Cdk5 in the cellular basis of sensory pain coding remain elusive. In addition, peripheral nociceptor activity is often studied using sensory nerve recordings in *ex vivo* tissue preparations, and technical barriers have limited *in vivo* investigation of the role of primary nociceptors and neuronal pain coding in sensitization and hyperalgesia. For example, cutaneous facial pain in response to light touch (hypersensitivity) needs more mechanistic characterization to define the neuronal signaling.

This study characterizes pain perception in the facial area of mice innervated by the TG maxillary nerve. We used intravital GCaMP6 calcium imaging to monitor TRPV1[lin] neurons to characterize the nature of TG signaling elicited by different modes of stimuli to compare the specificity or overlap of signaling. We also compared the effects of level of Cdk5 activity on this facial somatic sensing for different types of stimuli by examining alterations in calcium signaling and involvement of individual neurons. Finally, we tested whether a specific Cdk5 inhibitor could alleviate inflammation-induced hypersensitivity or hyperalgesia signaling from primary nociceptors. We discovered that enhanced Cdk5 activity in TG not only increased calcium influx in individual neurons, but also expanded the numbers of nociceptive cells responding to vibrissal pad noxious stimuli. In contrast, genetically decreased Cdk5 activity resulted in hyposensitivity. Notably, Cdk5 inhibitor application, either locally to the TG or by systemic administration, attenuated inflammation-induced nociceptor hyperactivity in the TG. These findings may have future translational impact by identifying a peripheral, rather than a CNS, therapeutic target for trigeminal facial inflammatory pain.

RESULTS

In vivo imaging of trigeminal ganglion nociceptor responses to facial mechanical, thermal, or chemical pain stimulation

We visualized trigeminal pain signaling directly using TRPV1-cre mice (Cavanaugh et al., 2011) crossed with Rosa26-CAG-flox-stop-GCaMP6f mice to genetically restrict expression

of the calcium indicator GCaMP6f to TRPV1[Lin] neurons. To monitor dynamic neuronal activities of the TG in real time as it responds to facial stimulation and pain, we adapted an intravital *in vivo* live-imaging technique (Ghitani et al., 2017) to expose the TG and optically record activity from large ensembles of genetically encoded primary sensory neurons (Figures 1A and 1B). TRPV1 channels are non-selective cation receptors gated by a broad array of noxious ligands. They act as polymodal receptors that can be independently activated by thermal, chemical, and mechanical stimulation (Cui et al., 2016). While live imaging the TG, we applied different stimuli in a standard sequence of mechanical, thermal, and chemical stimulation to the vibrissal pad to characterize the calcium-signaling responses of responding nociceptor populations. As expected, our results showed that TRPV1-GCaMP6f neurons respond to multiple forms of vibrissal pad stimulation, including mechanical (brush, von Frey hair [VF]), thermal (47°C), and chemical (capsaicin) stimuli. Each of these different modes of stimulation elicited a distinct response pattern (Figure 1C).

The application of non-noxious or noxious stimulation to the mouse vibrissal pad resulted in robust activation of discrete populations of TG neurons. Although some neurons responded to only one type of stimulation, indicating specificity, other populations of neurons exhibited polymodal sensitivity with nociceptive responses to two or more stimuli. Individual neurons displayed different combinations of response or non-response. For example, some neurons responded only to VF stimulation, others only to thermal, or only to capsaicin, yet some neurons were activated by brush as well as von Frey, or by thermal and capsaicin stimuli (Figure 1D).

Increased neuronal activities in Tgp35 mice in response to painful facial stimuli

We next compared the response of TRPV1[lin] neurons to different types of stimulation in wild-type mice compared with Tgp35 mice with elevated Cdk5 activity due to overexpression of p35 (Harada et al., 2001; Utreras et al., 2012). The different stimuli activated various ensembles of neurons while inducing different calcium signal encoding (Figure 2). Both brush (Figure 2A) and VF stimuli (Figure S1A) evoked a sharp calcium intensity peak, while both thermal (Figure S1B) and capsaicin (Figure 2B) stimuli produced more prolonged response times. To quantify the differences between mice, we quantified the number of activated neurons for each stimulus and calculated the area under the curve (AUC), which combines total fluorescence intensity with temporal response time. For brush stimulation, there were no significant differences in AUC measurements between Tgp35 and control mice; however, the number of activated neurons increased significantly (control 36.5 versus Tgp35 68, $p < 0.05$, Figure 2A). In contrast, in Tgp35 mice, VF stimuli produced larger AUC Ca^{2+} intensity values, while the activated neuronal population did not change (Figure S1A). With both 47°C thermal (Figure S1B) and capsaicin stimulation (Figure 2B) above the pain threshold applied to the mouse vibrissal pad, total calcium intensities increased significantly in Tgp35 mice, along with enhanced numbers of activated neurons compared with controls (capsaicin AUC, control 8.8 versus Tgp35 12.9, $p < 0.001$; capsaicin-activated neurons, control 41.2 versus Tgp35 61.7, $p < 0.05$). Together, these data indicate that Tgp35 mice with enhanced Cdk5 activity demonstrate increased pain stimulation of both total Ca^{2+} intensity and numbers of activated neurons. Moreover, these differences are stimulus dependent.

Decreased neuronal activities in p35 knockout mice in response to facial painful stimuli

Because of the substantial changes in neuronal firing/activity associated with Tgp35 mice, we next examined the neuronal responses of TRPV1^{lin} neurons in p35 knockout (KO) mice (previously established to have diminished Cdk5 activity) in response to the same stimuli. For brush stimulation, there were no statistically significant differences in either total calcium intensity or activated neuron number between p35 KO and control mice for this non-painful stimulus (Figure 2C). However, in response to VF stimulation, AUC Ca^{2+} intensities were significantly decreased in p35 KO mice, but the numbers of responding neurons remained similar (Figure S1C). Both thermal (Figure S1D) and capsaicin (Figure 2D) stimuli applied to the mouse vibrissal pad elicited decreased AUC Ca^{2+} intensities, as well as decreased total numbers of activated neurons (capsaicin AUC, control 10.2 versus KO 5.4, $p < 0.001$; neurons activated, control 59.2 versus KO 37.3, $p < 0.05$). These data, together with the findings from our Tgp35 mice, indicate a crucial role for the Cdk5-p35 pathway in regulating TG function in its response to noxious stimuli.

Specific versus polymodal TRPV1-lineage nociceptors in Tgp35 and p35 knockout mice

We next characterized the specific (firing in response to only a single stimulus) and polymodal (activation by two or more stimuli) neurons in TRPV1-GCaMP6f mice in response to noxious stimuli. Figure 3A illustrates these findings visually, showing color-coded merged images for the same microscope imaging field with various activated neurons responding to one, two, or three stimuli in Tgp35 mice. Venn diagrams (Figure 3B) for control and Tgp35 mice revealed altered proportions of neurons demonstrating a specific versus polymodal response. Tgp35 mice with elevated Cdk5 activity showed substantial increases in polymodal neurons in response to all noxious stimuli: 206%, 55%, and 240% increases in VF, thermal, and capsaicin stimuli, respectively (Figure 3C, chi-square test, $p < 0.05$). Enhanced Cdk5 activity also significantly decreased the proportion of specific neuronal nociceptor response to these three stimuli (Figure 3D). Total specific nociceptors were significantly decreased in Tgp35 mice (control 85% versus Tgp35 62%, chi-square test, $p < 0.05$), while the percentage of polymodal nociceptors correspondingly increased (control 15% versus Tgp35 38%, $p < 0.05$; Figure 3E). These data provide evidence that increased Cdk5 activity results in cross-excitation of specific nociceptors, which in turn increases the number of polymodal nociceptors. In p35 KO mice, however, the ratio of specific to polymodal nociceptors remained unchanged, i.e., no switch to increased specificity in response to any specific mode of pain stimulation (Figures S2A–S2E). Decreased Cdk5 activity affected only integrated Ca^{2+} intensity and had no effect on the activation of specific nociceptors and polymodal nociceptors. Phosphoproteomics analyses revealed that in mice with elevated Cdk5 activity, phosphorylation of cyclic AMP (cAMP)-PKA α and β catalytic subunits plus the sodium/calcium transporter Slc8a2 was increased (Figure S3E). We also confirmed increased TRPV1 phosphorylation in Tgp35 mice (Figure S3G).

Effects of TFP5 on complete Freund's adjuvant-induced inflammatory pain

Because Cdk5 activity enhances TG peripheral neuronal signaling, we tested whether a Cdk5 inhibitor can suppress inflammatory pain signaling at a peripheral site, rather than at

the CNS level. We used the classical complete Freund's adjuvant (CFA) mouse model for animal modeling of inflammatory pain with facial inflammatory hyperalgesia and allodynia (Krzyzanowska et al., 2011; McCarson, 2015). Each mouse first received an injection of 15 μL CFA into the vibrissal pad. After 6 or 24 h, live imaging was conducted to monitor neuronal responses after direct TFP5 peptide (80 mg/kg) application to the TG. Control CFA-induced inflammation mice showed a polymodal neuronal response to both non-noxious (brush) and noxious (capsaicin) stimulation representing inflammation-induced hyperalgesia. Figure 4A illustrates examples of color-coded activated neurons responding to capsaicin or brush stimulation after scrambled (Scb) control or TFP5 peptide treatment in CFA-induced inflammation mice. The amplitude of neuronal response to both brush and capsaicin decreased significantly after TFP5 treatment compared with the scrambled peptide control; moreover, AUC Ca^{2+} intensities also showed significant reductions after TFP5 application (Figures 4B and 4C). The number of neurons responding to both brush and capsaicin also decreased in TFP5-treated mice. The proportion of polymodal neurons increased dramatically in CFA mice compared with controls, but TFP5 treatment reduced it substantially (Figures 4D and 4E). Similar results were obtained by intraperitoneal administration of TFP5 (Figures S3A–S3D). Together, these data suggest that the Cdk5 inhibitor can downregulate the number of nociceptor neurons responding to both brush and capsaicin and decrease the magnitude of the integrated Ca^{2+} transients in response to both stimulations in inflamed mice. Thus, the Cdk5 inhibitor can alleviate inflammation-induced neuronal hypersensitivity, which contributes to mechanical hyperalgesia and allodynia.

DISCUSSION

In this study, we used intravital imaging in mice to compare dynamic TG neuronal signaling responses to four different stimuli. Key findings were that Cdk5 activity regulates both the intensity of Ca^{2+} signaling and its specificity. Inflammation significantly enhanced TG polymodal signaling, and a peptide inhibitor of Cdk5 suppressed both the intensity and the extent of polymodal signaling associated with inflammatory pain when administered either peripherally to the TG or intraperitoneally.

We characterized new patterns of specific and polymodal signaling in the TG in response to four different stimuli. Mechanical facial stimuli included light touch (brush) and pinch (VF), whereas noxious thermal stimulation was by direct contact to the vibrissal pad, and chemical noxious stimulation used capsaicin. Different stimulations induced distinct neuronal integrated calcium transients generally consistent with previous studies (Ghitani et al., 2017; Leijon et al., 2019).

We directly compared these modes of signaling in TRPV1lin neurons after modulating Cdk5 activity levels. Cdk5 regulated both the amplitude of pain signaling and the number of responding neurons. In contrast, altering Cdk5 activity had no apparent effect on the response to non-noxious mechanical stimulation, except for some increased numbers of responding neurons after Cdk5 hyperactivation. We discovered altered ratios of specific versus polymodal responses to all stimuli, i.e., more neurons exhibited signaling to more than one stimulus after elevation of Cdk5 activity.

Increased phosphorylation of cAMP-PKA and Slc8a2 could contribute to lower nociceptive thresholds and thus enhanced neuronal excitability (Aley and Levine, 1999; Eriksson et al., 2002; Taiwo et al., 1989; Taiwo and Levine, 1991). Elevated *in vivo* TRPV1 phosphorylation in Tgp35 mice also contributes to increased neuronal excitability. In addition, the voltage-gated T-type calcium channel regulators of neuronal activity, Cav3.1 (Calderón-Rivera et al., 2015) and Cav3.2 (Gomez et al., 2020), are also substrates of Cdk5, and they contribute to neuropathic pain (Cui et al., 2016). Cdk5 also regulates N-type calcium channels affecting presynaptic function (Brittain et al., 2012; Su et al., 2012). These channels might also contribute to Cdk5 regulation of trigeminal pain.

Our analyses characterized TRPV1 developmental lineage-labeled neurons regardless of TRPV1 channel expression in adulthood (McKemy, 2011), allowing us to examine neuronal populations broadly related to nociceptive modalities (Goswami et al., 2014). Enhanced Cdk5 activity could potentially influence sensory neuron properties at multiple levels, but our study establishes that it can change the modality responses of TG sensory neurons; e.g., genetic ablation of Cdk5 resulted in fewer responding neurons and less polymodal signaling when sensing thermal and noxious mechanical pain.

In a mouse model of facial inflammation, both separate and overlapping-modality Trpv1[lin] TG neurons were activated in response to noxious or previously non-noxious stimulation, consistent with previous studies (Amir and Devor, 2000; Tender et al., 2008). Compared with control mice, the percentage of polymodal nociceptor cell responses to brush and capsaicin stimuli increased dramatically from 0.02% to 40% (Figure 4E). This finding represents the first demonstration to our knowledge that at the level of TG calcium neuronal signaling, responses to noxious stimuli are enhanced, or pain is triggered by normally innocuous stimuli during inflammation. Smith-Edwards et al. (2016) demonstrated that inflammatory pain can shift the balance of sensory neuronal signaling in DRG, analogous to our findings. Peripheral inflammation induces increased Cdk5 activity (Pareek et al., 2006), and TRPV1 acts as a key receptor in nociceptive neurons whose function is strongly affected by Cdk5 phosphorylation, leading to hyperalgesia and allodynia (Jendryke et al., 2016; Liu et al., 2019; Simonic-Kocijan et al., 2013; Xing et al., 2012). Intrathecal administration of a Cdk5 inhibitor can alleviate inflammatory heat hyperalgesia in rats (Liu et al., 2015).

Here, we provide *in vivo* evidence that a Cdk5 inhibitor peptide, TFP5, can act directly on peripheral nerve pain signaling at the TG. Direct treatment of TG with TFP5 not only downregulated the polymodal nociceptor response to brush and capsaicin, but also decreased integrated calcium signaling for both stimuli. Virtually identical results were obtained by intraperitoneal injection of this inhibitor (Figures S3A–S3D). By suppressing pain signaling in peripheral TG neurons, inhibition of Cdk5 suppresses pain at the peripheral level.

Our study directly demonstrates the roles of Cdk5 activity in facial pain signaling in primary sensory neurons, suggesting an alternative approach to pain therapeutics. Targeting peripheral TG neurons could produce significant analgesic effects. This finding might ultimately have substantial translational impact, since most current pain medications are not selective for primary neurons and target multiple tissues, particularly the CNS, often

leading to serious side effects. Targeting Cdk5 activity at TG primary sensory neurons could offer better and safer treatments for facial pain.

Limitations of the study

We used epifluorescence microscopy to visualize GCaMP6 fluorescence, which limited the detection of fluorescence deep in the TG. In addition, we did not test whether TFP5 can cross the blood-brain barrier, so we cannot rule out possible CNS effects of TFP5.

STAR★METHODS

Detailed methods are provided in the online version of this paper and include the following:

RESOURCE AVAILABILITY

Lead contact—Further information and requests for resources and reagents should be directed to and will be fulfilled by the lead contact, Ashok Kulkarni Ashok.Kulkarni@nih.gov.

Materials availability—This study did not generate new unique reagents. For inquiries regarding the experimental material in this study, please contact the lead contact.

Data and code availability

- Original western blot images have been deposited at Mendeley and are publicly available as of the date of publication. The DOI is listed in the key resources table. Microscopy data reported in this paper will be shared by the lead contact upon request.

- All original code has been deposited at Zenodo and is publicly available as of the date of publication. DOIs are listed in the key resources table.

- Any additional information required to reanalyze the data reported in this paper is available from the lead contact upon request.

EXPERIMENTAL MODEL AND SUBJECT DETAILS

All mouse care and experimental procedures were approved by the Institutional Animal Care and Use Committee at the National Institute of Dental and Craniofacial Research, National Institutes of Health.

Animals—Mice were housed in a temperature- and light-controlled room ($23 \pm 2°C$ and 12 h light/dark cycle, respectively) with ad libitum food (2918 Teklad global 18% protein rodent diet, Envigo) and water. TRPV1-Cre (stock number 017769) and GCaMP6f (stock number 028865) strains were purchased from Jackson Laboratories. Mice with p35 knockout or transgenic overexpression, i.e., p35$^{-/-}$ background and Tgp35 mice, were generated in our laboratory (Pareek and Kulkarni, 2006). P35$^{-/-}$ mice were maintained in a C57BL6/129SVJ background. Tgp35 mice and wild-type littermate controls were maintained in an FVBN background. For imaging, mice were crossed to generate a GCaMP6 and TRPV1-Cre line, which was then maintained with p35$^{-/-}$ or tgp35

backgrounds. 78 mice were used (39 male and 39 female): C57BL6/129SVJ mice (JAX 000664, n = 18), TRPV1-Cre (+/−) GCaMP6(+/−) mice (n = 9), TRPV1-Cre (+/−) P35(−/−) GCaMP6 (+/−) mice (n = 9), TRPV1-Cre(+/−) GCaMP6(+/−)Tgp35 in FVBN background mice (n = 21) and TRPV1-Cre(+/−) GCaMP6(+/−) in FVBN background mice (n = 21). At the time of live imaging procedures, the mice were approximately 10–12 weeks old. For all experiments, age-matched wild-type littermates served as controls.

METHOD DETAILS

Surgery—Surgical procedures were conducted as described previously (Ghitani et al., 2017; Hu, 2019). In brief, mice at 8–10 weeks of age were anesthetized with inhalational Isoflurane (2%)/oxygen mix and positioned in a custom-built stereotactic frame with heads immobilized using ear bars. Continuous flow of isoflurane/oxygen was provided through a nosecone (Braintree Scientific, Inc.). Body temperature was maintained at $37°C \pm 0.5°C$ using a heat mat (CWE, Inc.), and temperature was monitored by a mouse rectal temperature probe throughout surgery and imaging. Under a dissecting stereoscope (Leica), scissors (Fine Science Tools) were used to remove skin from the top of the head, then connective tissue was removed to expose the skull, followed by partial decerebration surgery to obtain optical access to the trigeminal ganglion (Hu 2019). The cranium was repeatedly washed and bathed in HEPES buffer (160 mM NaCl, 6 mM KCl, 13 mM glucose, 13 mM HEPES, 2.5 mM $CaCl_2$, 2.5 mM $MgCl_2$ with pH adjusted to 7.2 using 10N NaOH). A rubber O-ring (9 mm diameter, RT Dygert) was glued over the opening in the skull using a cyanoacrylate-based adhesive. A custom-made stabilization bar securely mounted to the frame was attached to the O-ring and skull using dental cement.

Inflammation model—Mice were anesthetized with 2% isoflurane mixed with oxygen and were injected subcutaneously with 15 μL of complete Freund's adjuvant (CFA) solution (Sigma-Aldrich) (McCarson, 2015), or saline into the vibrissal pad using a 31-gauge needle (BD Ultra-Fine 6 mm needle). After 6 or 24 hours, live imaging was conducted to monitor neuronal responses after direct TFP5 peptide (80 mg/kg) application to the TG. After TFP5 application, brush stimulation was conducted first, and then 1 μM capsaicin was injected into the vibrissal pad of the mice. For the TFP5 treatment, the concentration of TFP5 was 20 mg/mL, and mouse weights ranged from ~20g to 30g. Accordingly, each mouse received ~80 to 120 μL TFP5.

Calcium imaging data collection and analysis—After surgery, the mouse was transferred to the stage of an epifluorescence inverted microscope (IX-71, Olympus) equipped with a 4X 0.28 NA air objective attached to an inverting device (LSM Technologies). Illumination was provided by a 130 W halogen light source (Olympus), using a standard GFP excitation/emission filter cube. Imaging was performed using an Orca Flash 4.0 CMOS camera (2016 Model, Hamamatsu), imaging at a 5 Hz frame rate, using Micro-Manager acquisition software to collect data.

Imaging data were analyzed using custom macro algorithms in ImageJ (NIH). For each field of view, the trigeminal ganglion V2 region (Edvinsson et al., 2020) was selected as region of interest for subsequent analyses. All image stacks were first aligned for motion correction

(MetaMorph, Molecular Devices). To identify neurons, maps of peak activity (maximal pixel intensity over mean pixel intensity) was median filtered, thresholded and separated by watershed segmentation to create regions of interest representing active neurons. A 2-pixel width ring around the circle were considered as local background. Fluorescence traces for each region of interest were subtracted from local background intensity.

Thermal, light touch, von Frey hair, and capsaicin stimulations—All stimuli were applied while the mouse was anesthetized and under continuous live imaging. For thermal stimulation, we use a copper tubing loop stimulator connected to a circulating water bath (LW Scientific, Italy). The temperature was maintained at 47.0°C (±0.5°C) to reach the hot nociceptive threshold. The stimulator was applied to the center of the right vibrissal pad of the mouse. Mechanical stimulation included both brush (light touch) and von Frey hair stimulation. Brush was performed using a cotton swab to gently brush the mouse right vibrissal pad. Von Frey hairs consisted of plastic monofilaments of equal length and varying diameters for which the force required to bend each filament was calibrated (Vos et al., 1994), We used 2g force von Frey filaments applied to the center of the right vibrissal pad.

We also examined the effects of 1 μM doses of capsaicin on TG neuronal activity. Capsaicin (Millipore Sigma) was injected subcutaneously through a 31-gauge needle (BD Ultra-Fine 6mm needle) into the center of the right vibrissal pad.

Protein sample preparation for two-dimensional electrophoresis—One group of trigeminal ganglions from Tgp35 and wildtype mice was homogenized in neuronal protein extraction reagent (N-PER, Thermo Fisher Scientific) containing protease (cOmplete Mini) and phosphatase (PhosSTOP) inhibitor cocktail tablets (both Roche, Indianapolis, IN). The second group of trigeminal ganglia was homogenized in N-PER containing only the protease inhibitor cocktail, and then treated with Lambda Protein Phosphatase (NEB) for 30min at 30°C. Total protein concentration was measured using a BCA Protein Assay Kit (Cat. No. 23227, Thermo Fisher Scientific). Samples were then sent to Kendrick Laboratories to perform 2D gel electrophoresis.

Two-dimensional electrophoresis—Two-dimensional electrophoresis was performed according to the carrier ampholyte method of isoelectric focusing by Kendrick Labs, Inc. (Madison, WI). Isoelectric focusing was carried out in a glass tube of inner diameter 2.3 mm using 2% pH 3–10 Isodalt Servalytes (Serva, Heidelberg, Germany) for 9,600 volt-hrs. One μg of an IEF internal standard, tropomyosin, was added to the sample. This protein migrates as a doublet with lower polypeptide spot of MW 33,000 and pI 5.2. The enclosed tube gel pH gradient plot for this set of Servalytes was determined with a surface pH electrode.

After equilibration for 10 min in Buffer 'O' (10% glycerol, 50 mM dithiothreitol, 2.3% SDS and 0.0625 M tris, pH 6.8), each tube gel was sealed to the top of a stacking gel that overlaid a 7% acrylamide slab gel (0.75 mm thick). SDS slab gel electrophoresis was carried out for about 4 h at 15 mA/gel. After slab gel electrophoresis, the gels for blotting were transferred to transfer buffer (10 mM CAPS, pH 11.0, 10% MeOH) and transblotted onto PVDF paper overnight at 200 mA and approximately 100 volts/two gels. The following proteins (MilliporeSigma) were added as molecular weight standards: myosin (220,000),

phosphorylase A (94,000), catalase (60,000), actin (43,000), carbonic anhydrase (29,000), and lysozyme (14,000). These standards appear as bands at the basic edge of the Coomassie Brilliant Blue R-250-stained PVDF membrane. The lower acid corner of the membrane has been marked with the page number of the blot.

Western blot—The membranes were wetted with 100% methanol and rinsed 4 times, 5 minutes each, in 100% methanol to destain the gels before western blotting. The membrane was then washed for 5 min in TBST (Tris Buffered Saline with 0.1% Tween-20; Quality Biological, 351-086-101; MilliporeSigma, P2287), non-specific sites were blocked in Blocking Solution (5% nonfat dry milk in TBST) for 1 h at room temperature (RT), incubated in anti-TRPV1 (VR1) antibody as the primary antibody diluted in Blocking Solution overnight at 4°C, washed 4 × 15 min with TBST at RT, incubated in LI-COR secondary antibodies diluted in Blocking Solution for 1–2 hours at RT, washed 4 × 15 min in TBST at RT, and imaged on a LI-COR Odyssey CLx imaging system controlled by LI-COR Image Studio software.

Sample preparation for phosphoproteomics—Trigeminal ganglion tissue from both Tgp35 and wildtype mice homogenates were lysed in 5% SDS in 10 mM sodium phosphate buffer, and then boiled for 2 minutes. Samples were clarified by centrifugation at 14,000g for 10min, and the supernatants were collected. Total protein concentration was measured using a BCA Protein Assay Kit. After reduction with TCEP and alkylation with iodoacetamide, proteins were digested with trypsin following the S-Trap digestion protocol (HaileMariam et al., 2018). The resulting tryptic peptides were dried under vacuum, labeled with TMTPro (A44520) following the manufacturer's protocol. 10% of each sample was set aside for analysis of background proteome and the remaining combined for phosphopeptide enrichment.

For phosphopeptide enrichment, we incorporated a 3-step sequential enrichment process: first with PTMScan from Cell Signaling Technology, followed by TiO2 enrichment, then Fe-NTA from Thermo Scientific. All steps followed the manufacturer's recommendations. 1 μg of enriched peptide from each step was analyzed, and after that the 3 fractions were combined and fractionated with the high pH fractionation kit from Thermo Scientific. Background proteome samples were combined and fractionated with the same protocol.

LC-MS/MS analysis—All fractions were analyzed by the same nanoLC-MS/MS method using a Thermo Scientific Fusion Lumos tribrid mass spectrometer interfaced to a UltiMate3000 RSLCnano HPLC system. For each analysis, 1 μg of the tryptic digest will be loaded and desalted in an Acclaim PepMap 100 trap column (75 μm × 2 cm) at 4 μL/min for 5 min. Peptides were then eluted into a 75 μm × 250 mm Acclaim PepMap 100 column (3 μm, 100 Å) and chromatographically separated using a binary solvent system consisting of A: 0.1% formic acid and B: 0.1% formic acid and 80% acetonitrile, at a flow rate of 300 nL/min. A gradient was run from 1% B to 42% B over 150 min, followed by a 5-min wash step with 80% B and a 10-min equilibration at 1% B before the next sample was injected. Precursor masses were detected in the Orbitrap at R = 120,000 (m/z 200). HCD fragment masses were detected in the orbitrap at R = 50,000 (m/z 200). Data-dependent MS/MS was carried out with top of speed setting, cycle time 2 s with dynamic exclusion of 20 s.

Proteomics data analysis—Protein identification and relative quantification were carried out using Proteome Discoverer software package (v2.5 Thermo Scientific). Raw data were searched against a Mus musculus proteome database from Protein Center along with a contaminant protein database with Sequest HT search engine, with PhosphoRS node for verification of phosphorylation sites. Up to 3 missed cleavages were allowed. Precursor mass was 10 ppm, fragment 0.02 Da. Carbomidomethylation on C and TMTPro on K and peptide N-terminus were set as static modifications, and M oxidation, N Q deamidation, and STY phosphorylation as dynamic modifications. For quantification, samples were normalized by total peptide abundance spectra with >50% isolation interference were excluded, Protein ratios were calculated based on pairwise ratios and hypothesis testing was by background-based t test.

QUANTIFICATION AND STATISTICAL ANALYSIS

All data are expressed as mean ± SEM, and n represents the number of mice analyzed; all replicates were biological replicates. The statistical evaluation was performed with GraphPad Prism 8 software (GraphPad, San Diego, CA). Statistical differences between the groups were assessed using a two-tailed unpaired *t* test with Welch's correction or chi-square test. A statistically significant difference was defined as $p < 0.05$. Error bars indicate SEM.

Supplementary Material

Refer to Web version on PubMed Central for supplementary material.

ACKNOWLEDGMENTS

REFERENCES

Aley KO, and Levine JD (1999). Role of protein kinase A in the maintenance of inflammatory pain. J. Neurosci. 19, 2181–2186. [PubMed: 10066271]

Amir R, and Devor M (2000). Functional cross-excitation between afferent A- and C-neurons in dorsal root ganglia. Neuroscience 95, 189–195. [PubMed: 10619475]

Bista P, and Imlach WL (2019). Pathological mechanisms and therapeutic targets for trigeminal neuropathic pain. Medicines (Basel) 6, 91.

Brittain JM, Wang Y, Eruvwetere O, and Khanna R (2012). Cdk5-mediated phosphorylation of CRMP-2 enhances its interaction with CaV2.2. FEBS Lett. 586, 3813–3818. [PubMed: 23022559]

Gomez K, Calderón-Rivera A, Sandoval A, González-Ramírez R, Vargas-Parada A, Ojeda-Alonso J, Granados-Soto V, Delgado-Lezama R, and Felix R (2020). Cdk5-Dependent Phosphorylation of Ca$_V$3.2 T-Type Channels: Possible Role in Nerve Ligation-Induced Neuropathic Allodynia and the Compound Action Potential in Primary Afferent C Fibers. J. Neurosci. 40, 283–296. [PubMed: 31744861]

Calderón-Rivera A, Sandoval A, González-Ramírez R, González-Billault C, and Felix R (2015). Regulation of neuronal cav3.1 channels by cyclin-dependent kinase 5 (Cdk5). PLoS ONE 10, e0119134. [PubMed: 25760945]

Cavanaugh DJ, Chesler AT, Braz JM, Shah NM, Julius D, and Basbaum AI (2011). Restriction of transient receptor potential vanilloid-1 to the peptidergic subset of primary afferent neurons follows its developmental downregulation in nonpeptidergic neurons. J. Neurosci. 31, 10119–10127. [PubMed: 21752988]

Cortes N, Guzman-Martinez L, Andrade V, Gonzalez A, and Maccioni RB (2019). CDK5: a unique CDK and its multiple roles in the nervous system. J. Alzheimers Dis. 68, 843–855. [PubMed: 30856110]

Crandall JA (2018). An introduction to orofacial pain. Dent. Clin. 62, 511–523.

Cui M, Gosu V, Basith S, Hong S, and Choi S (2016). Polymodal transient receptor potential vanilloid type 1 nocisensor: structure, modulators, and therapeutic applications. Adv. Protein Chem. Struct. Biol. 104, 81–125. [PubMed: 27038373]

Edvinsson JCA, Vigano A, Alekseeva A, Alieva E, Arruda R, De Luca C, D'Ettore N, Frattale I, Kurnukhina M, Macerola N, et al. (2020). The fifth cranial nerve in headaches. J. Headache Pain 21, 65. [PubMed: 32503421]

Eriksson KS, Sergeeva OA, Stevens DR, and Haas HL (2002). Neurotransmitter-induced activation of sodium-calcium exchange causes neuronal excitation. Ann. N. Y Acad. Sci. 976, 405–407. [PubMed: 12502587]

Ghitani N, Barik A, Szczot M, Thompson JH, Li C, Le Pichon CE, Krashes MJ, and Chesler AT (2017). Specialized mechanosensory nociceptors mediating rapid responses to hair pull. Neuron 95, 944–954 e944. [PubMed: 28817806]

Gonzalez-Ramirez R, Chen Y, Liedtke WB, and Morales-Lazaro SL (2017). TRP channels and pain. In Neurobiology of TRP Channels, Emir TLR, ed. (CRC Press/Taylor & Francis), pp. 125–147.

Goswami SC, Mishra SK, Maric D, Kaszas K, Gonnella GL, Clokie SJ, Kominsky HD, Gross JR, Keller JM, Mannes AJ, et al. (2014). Molecular signatures of mouse TRPV1-lineage neurons revealed by RNA-Seq transcriptome analysis. J. Pain 15, 1338–1359. [PubMed: 25281809]

HaileMariam M, Eguez RV, Singh H, Bekele S, Ameni G, Pieper R, and Yu Y (2018). S-trap, an ultrafast sample-preparation approach for shotgun proteomics. J. Proteome Res. 17, 2917–2924. [PubMed: 30114372]

Hall BE, Prochazkova M, Sapio MR, Minetos P, Kurochkina N, Binukumar BK, Amin ND, Terse A, Joseph J, Raithel SJ, et al. (2018). Phosphorylation of the transient receptor potential ankyrin 1 by cyclin-dependent kinase 5 affects chemo-nociception. Sci. Rep. 8, 1177. [PubMed: 29352128]

Harada T, Morooka T, Ogawa S, and Nishida E (2001). ERK induces p35, a neuron-specific activator of Cdk5, through induction of Egr1. Nat. Cell Biol. 3, 453–459. [PubMed: 11331872]

Hellmich MR, Pant HC, Wada E, and Battey JF (1992). Neuronal cdc2-like kinase: a cdc2-related protein kinase with predominantly neuronal expression. Proc. Natl. Acad. Sci. U S A 89, 10867–10871. [PubMed: 1279696]

Herrero Babiloni A, Guay S, Nixdorf DR, de Beaumont L, and Lavigne G (2018). Non-invasive brain stimulation in chronic orofacial pain: a systematic review. J. Pain Res. 11, 1445–1457. [PubMed: 30122975]

Hu M (2019). Visualization of trigeminal ganglion neuronal activities in mice. Curr. Protoc. Cell Biol. 83, e84. [PubMed: 30724481]

Jendryke T, Prochazkova M, Hall BE, Nordmann GC, Schladt M, Milenkovic VM, Kulkarni AB, and Wetzel CH (2016). TRPV1 function is modulated by Cdk5-mediated phosphorylation: insights into the molecular mechanism of nociception. Sci. Rep. 6, 22007. [PubMed: 26902776]

Julius D (2013). TRP channels and pain. Annu. Rev. Cell Dev Biol. 29, 355–384. [PubMed: 24099085]

Kim YS, Chu Y, Han L, Li M, Li Z, LaVinka PC, Sun S, Tang Z, Park K, Caterina MJ, et al. (2014). Central terminal sensitization of TRPV1 by descending serotonergic facilitation modulates chronic pain. Neuron 81, 873–887. [PubMed: 24462040]

Krzyzanowska A, Pittolo S, Cabrerizo M, Sanchez-Lopez J, Krishnasamy S, Venero C, and Avendano C (2011). Assessing nociceptive sensitivity in mouse models of inflammatory and neuropathic trigeminal pain. J. Neurosci. Methods 201, 46–54. [PubMed: 21782847]

Leijon SCM, Neves AF, Breza JM, Simon SA, Chaudhari N, and Roper SD (2019). Oral thermosensing by murine trigeminal neurons: modulation by capsaicin, menthol and mustard oil. J. Physiol. 597, 2045–2061. [PubMed: 30656684]

Liu J, Du J, and Wang Y (2019). CDK5 inhibits the clathrin-dependent internalization of TRPV1 by phosphorylating the clathrin adaptor protein AP2mu2. Sci. Signal. 12, eaaw2040. [PubMed: 31186372]

Liu J, Du J, Yang Y, and Wang Y (2015). Phosphorylation of TRPV1 by cyclin-dependent kinase 5 promotes TRPV1 surface localization, leading to inflammatory thermal hyperalgesia. Exp. Neurol. 273, 253–262. [PubMed: 26376215]

Liu SL, Wang C, Jiang T, Tan L, Xing A, and Yu JT (2016). The role of Cdk5 in alzheimer's disease. Mol. Neurobiol. 53, 4328–4342. [PubMed: 26227906]

McCarson KE (2015). Models of inflammation: carrageenan- or complete freund's adjuvant (CFA)-Induced edema and hypersensitivity in the rat. Curr. Protoc. Pharmacol. 70, 541–549.

McKemy DD (2011). A spicy family tree: TRPV1 and its thermoceptive and nociceptive lineage. EMBO J. 30, 453–455. [PubMed: 21285975]

Pareek TK, Keller J, Kesavapany S, Agarwal N, Kuner R, Pant HC, Iadarola MJ, Brady RO, and Kulkarni AB (2007). Cyclin-dependent kinase 5 modulates nociceptive signaling through direct phosphorylation of transient receptor potential vanilloid 1. Proc. Natl. Acad. Sci. U S A 104, 660–665. [PubMed: 17194758]

Pareek TK, Keller J, Kesavapany S, Pant HC, Iadarola MJ, Brady RO, and Kulkarni AB (2006). Cyclin-dependent kinase 5 activity regulates pain signaling. Proc. Natl. Acad. Sci. U S A 103, 791–796. [PubMed: 16407116]

Pareek TK, and Kulkarni AB (2006). Cdk5: a new player in pain signaling. Cell Cycle 5, 585–588. [PubMed: 16552189]

Pareek TK, Zipp L, and Letterio JJ (2013). Cdk5: an emerging kinase in pain signaling. Brain Disord. Ther. 2013, 003. [PubMed: 28316897]

Prochazkova M, Terse A, Amin ND, Hall B, Utreras E, Pant HC, and Kulkarni AB (2013). Activation of cyclin-dependent kinase 5 mediates orofacial mechanical hyperalgesia. Mol. Pain 9, 66. [PubMed: 24359609]

Rothermel M, Ng BS, Grabska-Barwinska A, Hatt H, and Jancke D (2011). Nasal chemosensory-stimulation evoked activity patterns in the rat trigeminal ganglion visualized by in vivo voltage-sensitive dye imaging. PLoS One 6, e26158. [PubMed: 22039441]

Schindelin J, Arganda-Carreras I, Frise E, Kaynig V, Longair M, Pietzsch T, Preibisch S, Rueden C, Saalfeld S, Schmid B, et al. (2012). Fiji: an open-source platform for biological-image analysis. Nat. Methods 9, 676–682. [PubMed: 22743772]

Simonic-Kocijan S, Zhao X, Liu W, Wu Y, Uhac I, and Wang K (2013). TRPV1 channel-mediated bilateral allodynia induced by unilateral masseter muscle inflammation in rats. Mol. Pain 9, 68. [PubMed: 24377488]

Smith-Edwards KM, DeBerry JJ, Saloman JL, Davis BM, and Woodbury CJ (2016). Profound alteration in cutaneous primary afferent activity produced by inflammatory mediators. Elife 5, e20527. [PubMed: 27805567]

Su SC, Seo J, Pan JQ, Samuels BA, Rudenko A, Ericsson M, Neve RL, Yue DT, and Tsai LH (2012). Regulation of N-type voltage-gated calcium channels and presynaptic function by cyclin-dependent kinase 5. Neuron 75, 675–687. [PubMed: 22920258]

Sugawara S, Shinoda M, Hayashi Y, Saito H, Asano S, Kubo A, Shibuta I, Furukawa A, Toyofuku A, and Iwata K (2019). Increase in IGF-1 expression in the injured infraorbital nerve and possible implications for orofacial neuropathic pain. Int. J. Mol. Sci. 20, 6360.

Taiwo YO, Bjerknes LK, Goetzl EJ, and Levine JD (1989). Mediation of primary afferent peripheral hyperalgesia by the cAMP second messenger system. Neuroscience 32, 577–580. [PubMed: 2557557]

Taiwo YO, and Levine JD (1991). Further confirmation of the role of adenyl cyclase and of cAMP-dependent protein kinase in primary afferent hyperalgesia. Neuroscience 44, 131–135. [PubMed: 1722888]

Takahashi S, Ohshima T, Cho A, Sreenath T, Iadarola MJ, Pant HC, Kim Y, Nairn AC, Brady RO, Greengard P, and Kulkarni AB (2005). Increased activity of cyclin-dependent kinase 5 leads to attenuation of cocaine-mediated dopamine signaling. Proc. Natl. Acad. Sci. USA 102, 1737–1742. [PubMed: 15665076]

Tender GC, Li YY, and Cui JG (2008). Vanilloid receptor 1-positive neurons mediate thermal hyperalgesia and tactile allodynia. Spine J. 8, 351–358. [PubMed: 18029293]

Utreras E, Keller J, Terse A, Prochazkova M, Iadarola MJ, and Kulkarni AB (2012). Transforming growth factor-beta1 regulates Cdk5 activity in primary sensory neurons. J. Biol. Chem. 287, 16917–16929. [PubMed: 22451679]

Vos BP, Strassman AM, and Maciewicz RJ (1994). Behavioral evidence of trigeminal neuropathic pain following chronic constriction injury to the rat's infraorbital nerve. J. Neurosci. 14, 2708–2723. [PubMed: 8182437]

Wang CH, Chou WY, Hung KS, Jawan B, Lu CN, Liu JK, Hung YP, and Lee TH (2005). Intrathecal administration of roscovitine inhibits Cdk5 activity and attenuates formalin-induced nociceptive response in rats. Acta Pharmacol. Sin. 26, 46–50. [PubMed: 15659113]

Wang CH, Lee TH, Tsai YJ, Liu JK, Chen YJ, Yang LC, and Lu CY (2004). Intrathecal cdk5 inhibitor, roscovitine, attenuates morphine antinociceptive tolerance in rats. Acta Pharmacol. Sin. 25, 1027–1030. [PubMed: 15301735]

Warwick CA, Shutov LP, Shepherd AJ, Mohapatra DP, and Usachev YM (2019). Mechanisms underlying mechanical sensitization induced by complement C5a: the roles of macrophages, TRPV1, and calcitonin gene-related peptide receptors. Pain 160, 702–711. [PubMed: 30507785]

Xing BM, Yang YR, Du JX, Chen HJ, Qi C, Huang ZH, Zhang Y, and Wang Y (2012). Cyclin-dependent kinase 5 controls TRPV1 membrane trafficking and the heat sensitivity of nociceptors through KIF13B. J. Neurosci. 32, 14709–14721. [PubMed: 23077056]

Yang YR, He Y, Zhang Y, Li Y, Li Y, Han Y, Zhu H, and Wang Y (2007). Activation of cyclin-dependent kinase 5 (Cdk5) in primary sensory and dorsal horn neurons by peripheral inflammation contributes to heat hyperalgesia. Pain 127, 109–120. [PubMed: 16996690]

Highlights

- Characterization of calcium signaling in trigeminal ganglion using *in vivo* live imaging

- Cdk5 activity regulates trigeminal peripheral neuronal pain signaling

- Elevated Cdk5 activity increases the proportion of polymodal nociceptors

- A Cdk5 inhibitor alleviates inflammation-induced trigeminal hyperalgesia signaling
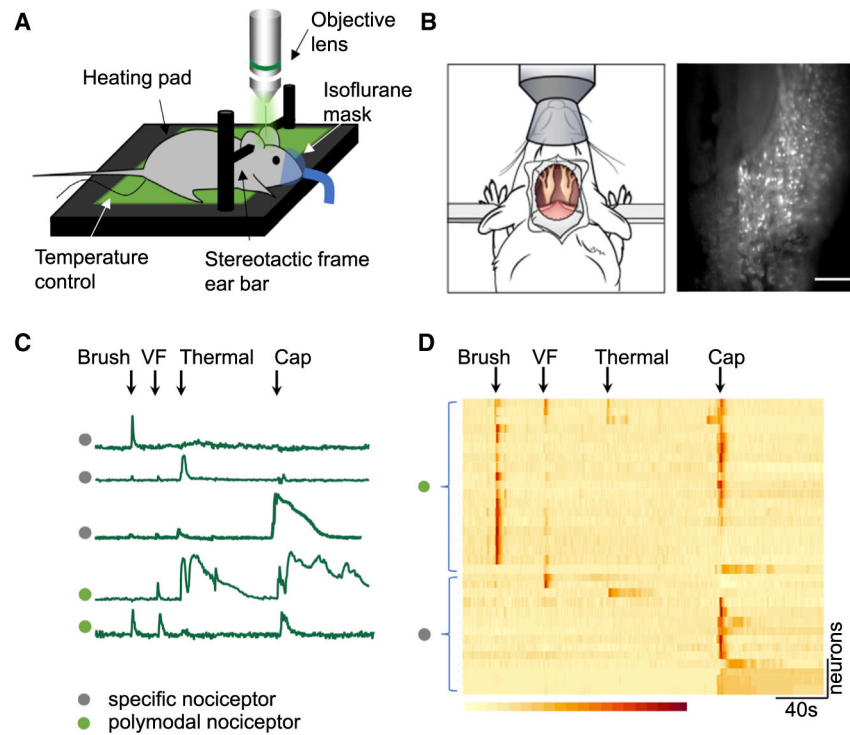
Figure 1. *In vivo* imaging of the trigeminal ganglia (TG) in response to different modes of vibrissal pad pain stimulation

(A) Diagram of the surgical mount and imaging system prior to exposing the mouse TG.

(B) A top-down view of the mouse surgical preparation with exposed TG (left), visualizing Ca^{2+} responses induced by pinch stimulation (right). Scale bar, 500 μm.

(C) Ca^{2+} intensity traces for different types of nociceptors during live imaging. The first three traces represent specific nociceptor responses to brush, thermal (47°C), or capsaicin stimuli, respectively. The bottom two Ca^{2+} traces illustrate polymodal responses. VF, von Frey hair fiber; Cap, capsaicin.

(D) Heatmap showing the four types of responses by TRPV1-GCaMP6 trigeminal neurons to brush, VF pinch, thermal, and capsaicin stimuli collected sequentially in each mouse. Color scale indicates the changes in calcium imaging intensity (F/F).
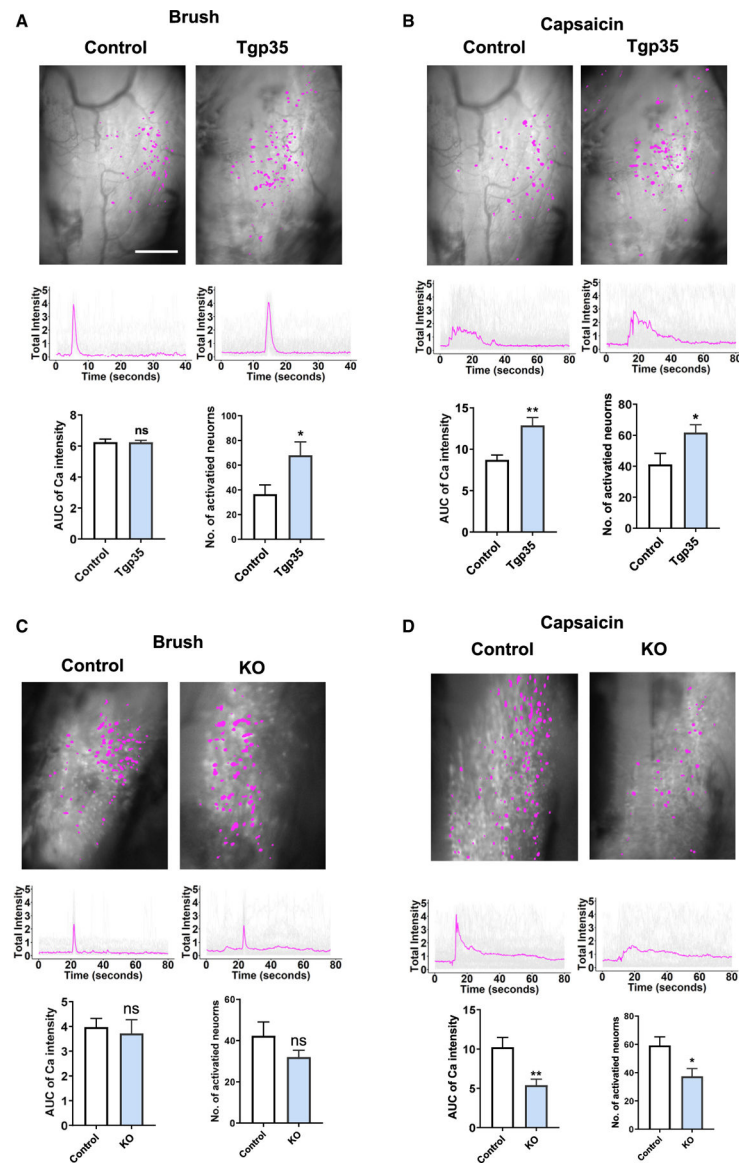
Figure 2. TG sensory neuronal responses to vibrissal pad brush, von Frey hair, thermal, or capsaicin stimulation in Tgp35 and p35 knockout (KO) mice

(A) Top: representative imaging fields of TG TRPV1-GCaMP6-expressing neurons responding to brush in control or Tgp35 mice. Middle: representative calcium traces in response to brush stimulation in individual mice, showing typical response profiles. Gray lines are traces from each TG neuron; magenta line shows the mean value for these traces. Lower left: comparison of AUCs of calcium traces from control and Tgp35 mice in response to brush, showing no significant difference (ns) in responses to this stimulation. Lower right: numbers of neurons activated by this stimulation, showing significantly more neurons responding in Tgp35 compared with control mice (n = 6 mice). AUC, area under the curve; the data represent mean ± SEM, *p < 0.05, **p < 0.001; scale bar, 500 μm.

(B) For capsaicin stimulation, both AUCs and numbers of activated neurons substantially increase in Tgp35 mice compared with wild-type mice.

(C) Representative images of neurons responding to brush stimulation in control versus KO mice. Bottom left: no significant difference in AUCs in response to brush stimulation. Bottom right: numbers of activated neurons show a decreasing, non-significant trend in KO compared with control mice (n = 6).

(D) For capsaicin stimulation, both AUCs and numbers of activated neurons substantially decrease in KO mice compared with wild-type mice.
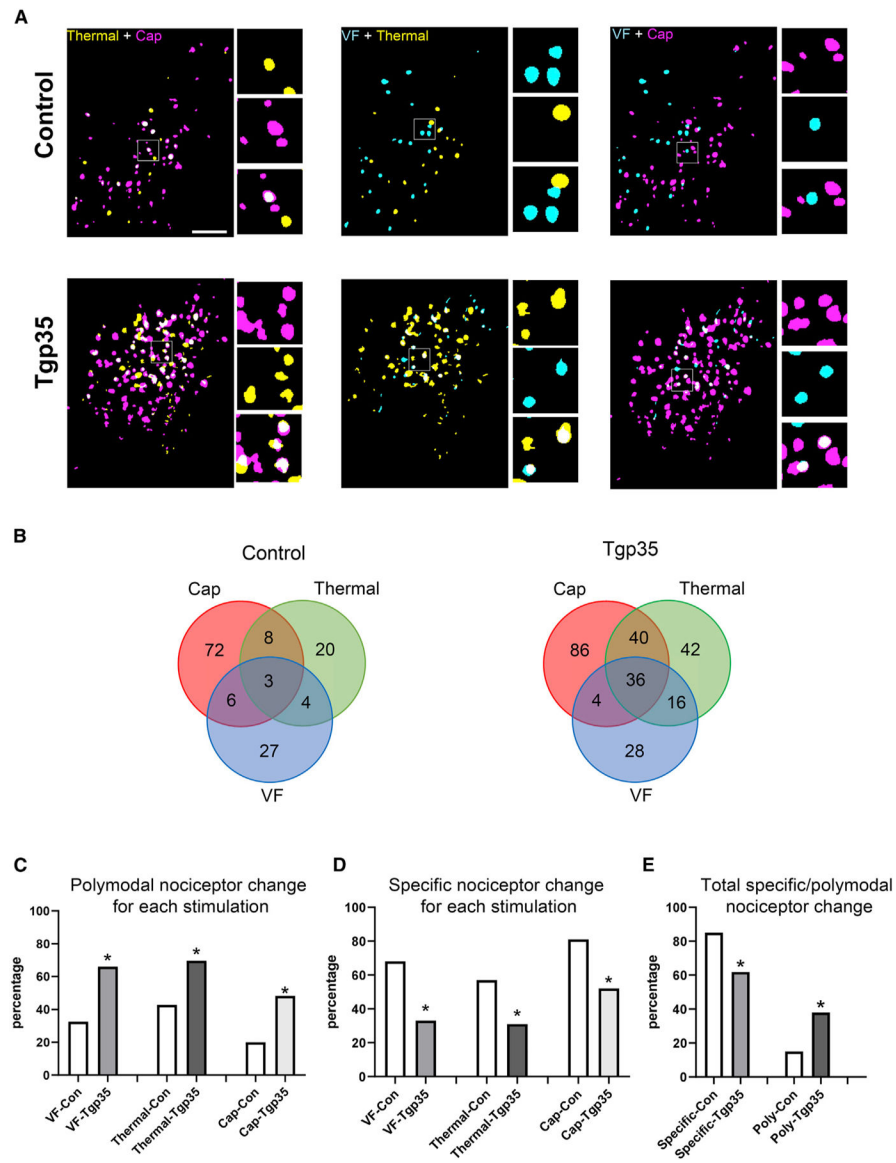
Figure 3. Altered distribution of polymodal sensory neuron signaling in TG of Tgp35 mice

(A) Representation of specific and polymodal neuron activation in Tgp35 mice. Left: color-coded map of representative fields showing distribution of neurons activated by either capsaicin (magenta) or thermal (yellow) or both stimuli (white) in control versus Tgp35 mice. Insets: magnified views of white-boxed regions. Middle and right: color-coded maps of neuron distributions responding to von Frey hair (VF, cyan) versus thermal (yellow) or capsaicin (red) stimulation; white indicates overlap. Scale bar, 500 μm.

(B) Venn diagrams identifying numbers of specific versus polymodal (overlapping circles) TRPV1^{lin} TG neurons responding to VF (blue), thermal (green), or capsaicin (red) stimuli; n = 3 mice, 392 neurons.

(C) Percentage change of polymodal neurons for VF, thermal, or capsaicin stimulation showing significant increases in polymodal nociceptors for each stimulation.

(D) Percentage change of specific nociceptor neurons responding to VF, thermal, or capsaicin showing significantly decreased neuronal response to these stimuli compared with control mice by chi-square test.

(E) Altered percentages of specific versus polymodal nociceptor neurons responding to sequential von Frey mechanical, thermal, and capsaicin stimulation in control versus Tgp35 mice. *p < 0.05.
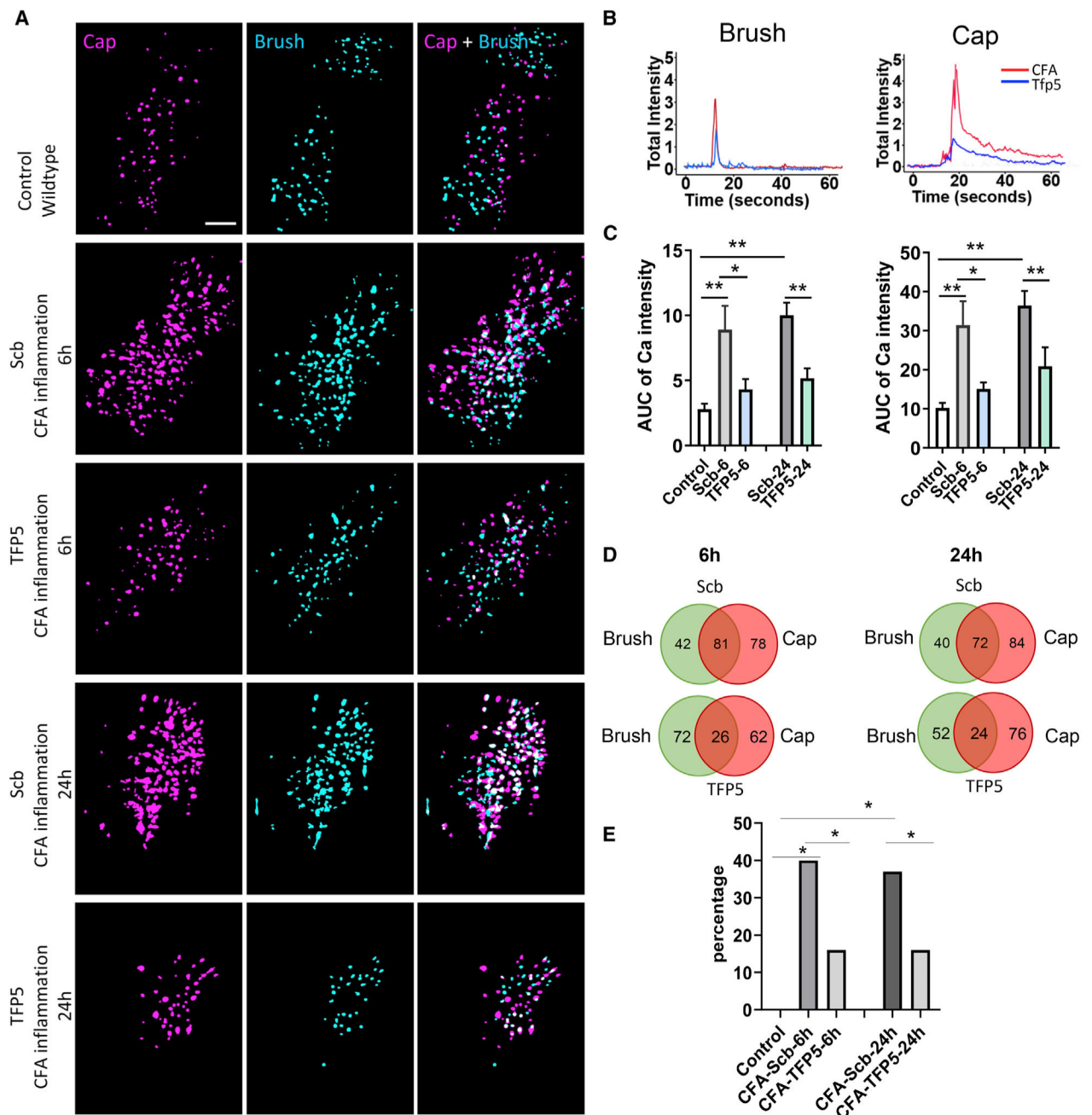
Figure 4. Effects of direct application of the Cdk5 inhibitor TFP5 to trigeminal ganglia on neuronal responses to vibrissal pad brush and capsaicin in mice with vibrissal pad inflammation

(A) Representative color-coded maps of neuronal responses to capsaicin (magenta) and brush (cyan) stimulation in scrambled (Scb) control peptide- and TFP5-treated mice 6 and 24 h after CFA injection to induce inflammation. Right: merge of the two stimulations, where white indicates overlap. Scale bar, 500 μm.

(B) Representative calcium traces responding to brush or capsaicin stimulation in TG treated with Scb control or TFP5 peptides.

(C) Quantification of AUCs for both stimulations in Scb and TFP5 mice with a substantial decrease after TFP5 treatment compared with the Scb (scrambled) peptide control at 6 and 24 h time points.

(D) Venn diagrams showing distributions of specific and polymodal neuronal responses to brush and capsaicin stimulation at 6 h (n = 3 mice, 361 neurons) and 24 h (n = 3 mice, 348 neurons) time points.

(E) Percentage above controls of polymodal nociceptors responding to both brush and capsaicin stimulation at 6 and 24 h time points. Polymodal nociceptors are dramatically increased both 6 and 24 h after CFA-induced inflammation in the vibrissal pad, with a significant decrease after TFP5 treatment. $*p < 0.05$, $**p < 0.001$.

KEY RESOURCES TABLE

REAGENT or RESOURCE	SOURCE	IDENTIFIER
Antibodies		
Anti-TRPV1 (VR1) Antibody	Alomone labs	Cat #: ACC-030; RRID:AB_2313819
680RD goat anti-rabbit	LI-COR	926-68071; RRID: AB_10956166
N-PER™ Neuronal Protein Extraction Reagent	Thermo Fisher Scientific	PI87792
Lambda Protein Phosphatase (Lambda PP)	New England Biolabs	P0753L
Chemicals, peptides, and recombinant proteins		
Capsaicin	Millipore Sigma	M2028
Freund's Adjuvant, Complete	Millipore Sigma	F5881
Scramble peptide for TFP5	GenScript	GGGFWDRCLSGKGKMSSKGGGINAYARAARRAARR
TFP5	GenScript	KEAFWDRCLSVINLMSSKMLQINAYARAARRAARR
Experimental models: Organisms/strains		
Mouse: B6J.Cg-Gt(ROSA)^{26Sortm95.1(CAG-GCaMP6f)Hze}/MwarJ	The Jackson Laboratory	Stock no.: 028865
B6.129-Trpv1tm1^{(cre)Bbm}/J	The Jackson Laboratory	Stock no.: 017769
Mouse: Tgp35	NIDCR, NIH	Takahashi et al., 2005
Mouse: TRPV1-Cre/GcAMP6/Tgp35	This paper	N/A
Mouse: TRPV1-Cre/GcAMP6f/p35	This paper	N/A
Software and algorithms		
ImageJ (Fiji)	Schindelin et al., 2012	https://fiji.sc
GraphPad	GraphPad Software	https://www.graphpad.com/
MetaMorph	Molecular Devices	https://www.moleculardevices.com/products/cellular-imaging-systems/acquisition-and-analysis-software/metamorph-microscopy#gref
Custom code to analyze images	This paper	GitHub: 10.5281/zenodo.5998544
Other		
PTMScan Phospho-Enrichment IMAC Fe-NTA Magnetic Beads	Cell Signaling Technology	20432
High-Select TiO$_2$ Phosphopeptide Enrichment Kit	Thermo Scientific	A32993
High-Select Fe-NTA Phosphopeptide Enrichment Kit	Thermo Scientific	A32992
S-Trap Micro kit	ProtiFi	K02-micro-10
Original western blot images	This paper	Mendeley Data: 10.17632/9x8g8m45br.1